

Dynamic Screening of the Core Exciton by Swift Electrons in Electron-Energy-Loss Scattering

P. E. Batson and J. Bruley^(a)

IBM Thomas J. Watson Research Center, Yorktown Heights, New York 10598

(Received 10 September 1990; revised manuscript received 7 January 1991)

We show for the first time that electron-energy-loss measurements of atomic absorption are different from the soft-x-ray photoyield data in the region influenced by the core exciton. We suggest that the core-exciton envelope function is influenced by the swift electron and its associated charge-density wake. Solving Schrödinger's equation for a model transition potential including the swift electron, we find that the observed differences for SiO_x, diamond, and Si can be reproduced. Spectra from aluminum are included as a comparison when the exciton is absent.

PACS numbers: 71.45.Gm, 71.35.+z, 78.90.+t

In the sudden limit, it is well known that inelastic scattering of a swift electron by core excitations is obtained from a generalization of the dipole-allowed photoabsorption [1]. In this limit the swift electron passes beyond some excitation volume well before the perturbed system begins to evolve into an excited state. Otherwise, the final state may be distorted by the swift electron. In semiconductors, core-excitation spectra are often dominated by a Wannier exciton having an orbital radius of a few angstroms. If the swift electron does not pass beyond the exciton radius well before the transition is complete, we suggest that the exciton will be distorted, leading to a breakdown of the conventional approach. This leads to observable differences between the energy-loss and photoabsorption results even for the soft-x-ray edges, where it has been assumed that the sudden limit is very good.

In Fig. 1, we examine the carbon 1s absorption in diamond, comparing the electron-energy-loss spectroscopy (EELS) results with the soft-x-ray partial photoyield (PY) data from Morar *et al.* [2]. The EELS data were collected under conditions which satisfy the dipole limit.

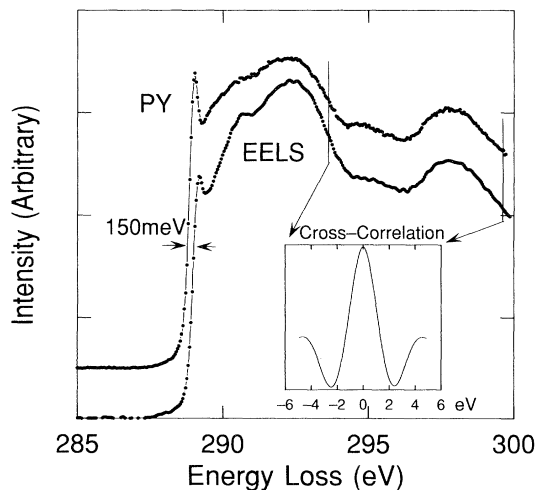


FIG. 1. Comparison of EELS and photoyield (PY) results for the carbon 1s excitation in diamond. Inset: Cross correlation of the data from 294 to 300 eV. Differences are confined to the near-edge region.

Beyond about 4 eV from the edge, the spectra are identical. To quantify this, we include in the inset a cross correlation of the two sets of data from 294 to 300 eV. Near onset, the core exciton is weaker in the EELS case, the onset energy is different by 150 meV, and the slope of the continuum is larger.

To understand this behavior, we have used the exciton formalism developed by Elliott [3], and extended by Altarelli and Dexter [4]. In that analysis, the core hole is created suddenly. Subsequently, the perturbing photon (or electron) field causes a transition from a ground-state core level to an excitonic state calculated in the presence of the statically screened core hole. We follow this approach by assuming a sudden creation of both the core hole and a swift electron at the origin. We then calculate an excitonic envelope function in the presence of a total potential due to the core hole plus a time-averaged fraction of the swift electron during the transition. The exciton solutions are distorted, their mean energies are shifted, and the scattering intensity is modified. This does not alter the set of Bloch functions used to make up the exciton orbitals, but instead redistributes scattering intensity among them [4,5]. This simplification of the time-varying nature of the swift electron potential is similar to the use of a phenomenological transition potential [6] to calculate final-state configurations.

When a swift electron penetrates matter, a longitudinal charge-density wake is also induced [7,8]. This consists of a trailing correlation hole and small leading density fluctuations. At large distances, the correlation hole collapses, initiating a plasmon excitation. Even at distances of order 0.5–1.0 nm, the wake can dominate the total potential. Thus, we suggest that to model the EELS results, we must include the wake in the exciton analysis. Unfortunately, full expressions for the charge-density wake, derived in detail by Echenique, Ritchie, and Brandt [8], are very complicated. Therefore we have used a model potential which embodies in a simplified way the symmetry of the swift electron plus the wake. In the parabolic coordinate system defined by [9] $x = (\lambda\mu)^{1/2} \cos\phi$, $y = (\lambda\mu)^{1/2} \sin\phi$, $z = \frac{1}{2}(\lambda - \mu)$, we consider the potential energy

$$V = -\frac{|e|^2}{er} [1 - \alpha(1 + \eta\mu + \xi\lambda)]. \quad (1)$$

In this model the swift electron is located at the origin, and is traveling in the positive z direction. The first term is the usual potential for a core hole screened by the bulk dielectric constant ϵ . The second term describes (1) a swift electron having a strength which is some fraction α of the screened-hole potential, (2) a trailing correlation hole of strength $-\eta$ relative to the swift electron, and (3) a leading density fluctuation of strength ξ . The parameters η and ξ have dimensions of inverse length. In Fig. 2, on the right, we show an intensity plot of the total potential for $\alpha=0.6$, $\eta=-0.008$, and $\xi=0.0$, and materials properties appropriate to silicon, as summarized in Table I. On the left, we show the screened-core-hole potential alone with $\alpha=0$. It can be seen that the potential is made less deep due to the presence of the swift electron, and is distorted towards $-z$ due to the trailing correlation hole.

With this potential, the Schrödinger-like equation for exciton bound and continuum envelope functions is solvable analytically in the effective-mass approximation. We then obtain closed-form solutions for the exciton envelopes at the origin as a function of the parameters α , η , and ξ . Finally, the excitonic spectrum is calculated and compared with experiment. This calculation is straightforward and will be covered elsewhere. In Fig. 2, we show the model results for the contour at half height of the first excitonic bound state in silicon without (left) and with (right) the swift electron. On the left, the Elliott result is recovered. On the right, the bound-state orbital is larger, and is elongated in the $-z$ direction by the presence of the correlation hole. The bound-state energy has

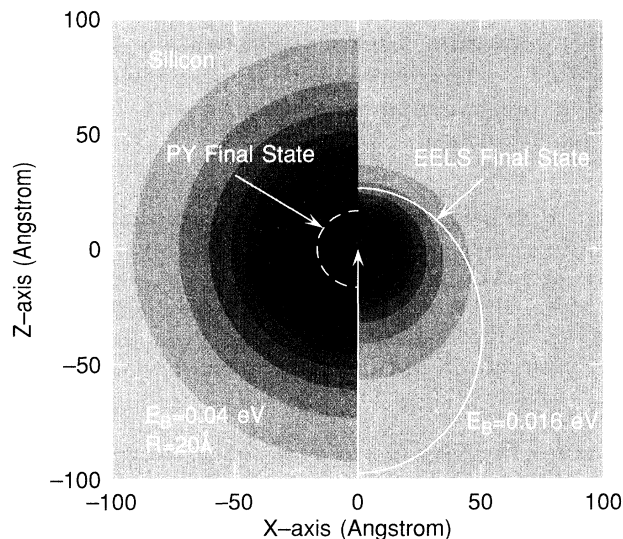


FIG. 2. Composite contour plot of total potential well with the swift electron (right) and without (left). The contours at half height for the first bound-state orbitals are shown as white lines. In the presence of the swift electron and wake, the orbital is larger and distorted towards the trailing correlation hole.

TABLE I. Summary of materials parameters: diamond from Ref. [2], silicon from Ref. [4], and SiO_x from Ref. [15] (except Γ which is larger, reflecting the disordered nature of these samples). E_b is the exciton binding energy for photoabsorption. E_{CB} is the conduction-band edge energy. Γ is the exciton damping energy. ΔE is the energy resolution.

	ϵ	E_b	E_{CB}	Γ	ΔE
SiO_x	2	1.400	107.05	0.62	0.350
Diamond	5.7	0.189	289.18	0.17	0.225
Silicon	11.7	0.040	99.86	0.10	0.240
Aluminum	$-\infty$	0.000	72.72	\dots	0.160

been shifted to 16 meV from the Elliott value of 40 meV.

The EELS results for natural diamond were obtained from electron-transparent areas at the edges of unthinned powders. Results for silicon were obtained in 50-nm-thick ion-milled single-crystal silicon (p -type, $4 \times 10^{12} \text{ cm}^{-3}$ boron doped). Spectra for SiO_x were obtained from material grown at low temperature by a chemical-vapor-deposition process. Aluminum data were obtained from 50-nm films evaporated onto NaCl. The EELS instrument was the VG Microscopes HB501 scanning transmission electron microscope fitted with a high-energy-resolution electron spectrometer [10]. The electron probe size was nominally 1 nm at 100 keV. The energy distribution of electrons emitted by the field-emission tip closely followed a Fowler-Nordheim distribution with a width of 0.4 eV. We used the presence of the sharp Fermi tail on the high-energy side of this distribution to allow an unfolding of the field-emission shape from the data to give Gaussian spectral resolutions as shown in Table I. The absolute accuracy of the energy-loss scale in these measurements was ± 20 meV. The PY results were accurate to about ± 50 meV as quoted by others for diamond and silicon. For aluminum, the x-ray-absorption results were accurate to about ± 20 meV. For the native-oxide PY results, the presence of a Si substrate signal allowed an accurate calibration to ± 50 meV.

In Fig. 3, we summarize comparisons of EELS and PY data for SiO_x , diamond, and silicon, and x-ray-absorption (XAS) data for aluminum. The data have been shifted to align the conduction-band (CB) edges shown in Table I. The Al results demonstrate that, when the exciton is absent, the XAS data [11] match the EELS data to within a ± 20 -meV accuracy at 0.160-meV resolution.

For diamond, we reproduce the PY Elliott fit using $\alpha=0$ and parameters from the prior work [2], summarized in Table I. Next, we let $\alpha=0.3$, effectively reducing the exciton binding energy to 0.090 eV (dashed line). The edge position shifts by 150 meV, but the exciton peak is not resolved at this energy resolution and damping. Finally, by letting η and ξ be nonzero, we find that the exciton becomes more tightly bound and its intensity

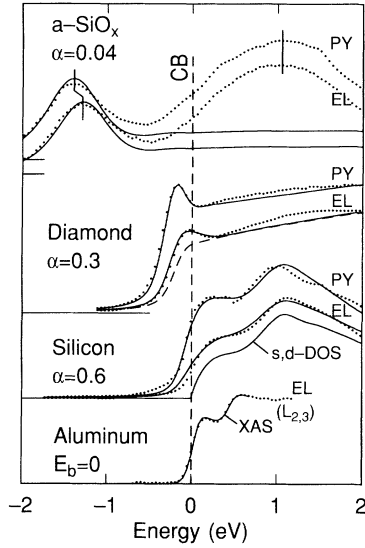


FIG. 3. Comparison of photoyield (PY) and EELS (EL) results for SiO_x , diamond, and silicon, and x-ray absorption (XAS) for aluminum. The data have been shifted to align conduction-band edges (CB). Fits to the PY data are standard Elliott solutions using the materials parameters of Table I. Fits to the EL data use the additional parameters from Table II. Omission of the wake ($\eta=0$) in the diamond case produces the dashed line. The aluminum results are identical for the XAS (solid line) and EL (dotted line) cases.

increases. The best fit is obtained with $\eta = -0.05 \pm 0.003$ and $\xi = 0.012 \pm 0.001$. These parameters support the notion that the dominant wake contribution should be due to a trailing correlation hole ($\eta < 0$).

For silicon, we compare the L_3 edge with PY results from Eberhardt *et al.* [12]. The L_3 intensity has been extracted from the $L_{2,3}$ data assuming a 0.608-eV spin-orbit splitting and a 2:1 branching ratio [13]. We use the Elliott-theory parameters from Table I, originally given by Altarelli and Dexter [4], and an iterative procedure to obtain a final density of states (s,d DOS), α , η , and ξ which are consistent with both the PY and the EELS data. We find $\alpha = 0.60 \pm 0.05$, $\eta \approx -0.008$, $\xi \approx 0.00$. We can see that the EELS result follows the DOS closely, while the PY measurement is distorted near the threshold, and shifted to lower energy by the exciton.

For SiO_x we compare with recent native-oxide PY data [14]. With appropriate background stripping to eliminate the Si substrate signal, the PY and the EELS data overlapped almost perfectly. The L_3 edge was then extracted using a spin-orbit splitting of 0.608 eV and a 0.7:1 branching ratio as found by others [14,15]. This edge consists of three peaks—an exciton at 1.4 eV below CB, a second peak 1.05 eV above CB, and a third peak about 8 eV above CB. The second and third peaks are aligned to within the accuracy of the measurements (± 50 meV). The exciton peaks, however, do not align well, with the EELS result being about 0.1 eV higher in

energy. Using the materials parameters from Table I, similar to those obtained in Ref. [15], we can reproduce the PY exciton position with $\alpha=0$ and the EELS position with $\alpha=0.04$. The EELS results are not sensitive to η because the exciton is so tightly bound.

We can estimate α by speculating that it might be proportional to the fraction f of the transition time that the swift electron remains within the exciton orbit radius. If we assume that during the transition the core electron expands with a velocity v_{core} determined by its momentum uncertainty in the core orbital, then $f = v_{\text{core}}/v_0$ and we have

$$\alpha_{\text{th}} \equiv \varepsilon f \approx \varepsilon \frac{v_{\text{core}}}{v_0} \approx \varepsilon \frac{1}{v_0} \frac{\hbar}{m a_0} E_{\text{core}}^{1/2}, \quad (2)$$

where a_0 is the Bohr radius, E_{core} is the core-electron binding energy given in rydbergs, and v_0 is the swift-electron velocity. Thus, α summarizes the time-averaged strength of the swift-electron potential relative to the statically screened hole potential. If ε is small, the hole potential is deep, α is small, and the Elliott exciton results are recovered. If ε is large, the hole potential is weak, α is large, and the core exciton is distorted. In Table II, we show calculated values of α compared to those obtained from the fits above. The order of magnitude and relative trend with material is reproduced. This result is simply a restatement of the general criterion for the validity of the sudden limit—that the swift-particle velocity be much bigger than the core orbital velocity. But in this case the weak energetics of the exciton state force a more stringent requirement, leading to a breakdown of the sudden limit even for the soft-x-ray edges.

An estimate for η can be found by reference to the work of Echenique, Ritchie, and Brandt [8]. This is just proportional to the wake potential at the origin:

$$\eta \equiv \lim_{r \rightarrow 0} \frac{1}{e} \left(\Phi_{\text{tot}} - \frac{e}{r} \right) = -\frac{\pi}{2} \frac{\omega_p}{v_0}, \quad (3)$$

where ω_p is the plasma frequency. Results for the examples above are given in Table II. Estimates for ξ , the single-particle charge-density fluctuations, are of order 1% of η . The larger value needed for diamond is probably due to the nonideal shape of the model potential. In Fig. 2, we see that the Elliott excitonic envelope becomes

TABLE II. Comparison of swift-electron strength parameter α and wake strengths η, ξ from model fits with predictions of Eqs. (2) and (3). η and ξ are in units of \AA^{-1} .

	α_{fit}	α_{theory}	η_{fit}	η_{theory}	ξ_{fit}	ξ_{theory}
SiO_x	0.04	0.08	a	-0.027	a	0.0
Diamond	0.30	0.40	-0.050	-0.056	0.012	0.0
Silicon	0.60	0.49	-0.008	-0.028	0.000	0.0

^aThis fit was not sensitive to η or ξ .

larger both in the lateral (x,y) and longitudinal (z) directions. But the correct wake potential is much narrower in the lateral dimensions than the simple model. Thus, we expect the correct envelope to be narrower than that shown in Fig 2. This should increase the envelope intensity at the origin, enhancing the exciton intensity. Positive values of ξ also push the envelope solutions closer to the origin, so an incorrect envelope intensity can be adjusted by allowing ξ to be nonzero. Therefore, Fig. 2 summarizes the qualitative, rather than quantitative, behavior of this scattering situation.

These results show for the first time experimentally that the EELS and PY results are different at the level required for interpretation of near-edge fine structure. The new understanding implies that EELS spectra for some materials, notably silicon, resemble the conduction-band DOS very closely, but this is not to say that excitonic interactions may be neglected altogether. The model calculation is speculative, simplistic, and qualitative, but we believe that it captures the controlling physics of the process—a failure of the sudden limit for scattering brought about by the very weak energetics of typical core excitons in the semiconductors.

We thank P. M. Echenique for several informative conversations.

^(a)Present address: Max Planck Institute, Seestrasse 92, D-

7000 Stuttgart, Germany.

- [1] M. Inokuti, *Rev. Mod. Phys.* **43**, 297 (1971).
- [2] J. F. Morar, F. J. Himpsel, G. Hollinger, G. Hughes, and J. L. Jordan, *Phys. Rev. Lett.* **54**, 1960 (1985).
- [3] R. J. Elliott, *Phys. Rev.* **108**, 1384 (1957).
- [4] M. Altarelli and D. L. Dexter, *Phys. Rev. Lett.* **29**, 1100 (1972).
- [5] G. D. Mahan, *Many-Particle Physics* (Plenum, New York, 1981), pp. 738–743.
- [6] For instance, A. Zunger, *Phys. Rev. Lett.* **50**, 1215 (1983).
- [7] V. N. Neelavathi, R. H. Ritchie, and W. Brandt, *Phys. Rev. Lett.* **33**, 302 (1974).
- [8] P. M. Echenique, R. H. Ritchie, and W. Brandt, *Phys. Rev. B* **20**, 2567 (1979).
- [9] P. M. Morse and H. Feshbach, *Methods of Theoretical Physics* (McGraw-Hill, New York, 1953), Vol. II, p. 1667.
- [10] P. E. Batson, *Rev. Sci. Instrum.* **57**, 43 (1986); **59**, 1132 (1988).
- [11] C. G. Olson and D. W. Lynch, *Solid State Commun.* **31**, 601 (1979).
- [12] W. Eberhardt, G. Kalkoffen, C. Kunz, D. Aspnes, and M. Cardona, *Phys. Status Solidi (b)* **88**, 135 (1978).
- [13] F. C. Brown and O. P. Rustgi, *Phys. Rev. Lett.* **28**, 497 (1972).
- [14] Curve *B* of Fig. 4 in G. R. Harp, Z. L. Han, and B. P. Tonner, *Phys. Scr.* **T31**, 23 (1990).
- [15] V. J. Nithianandam and S. E. Schnatterly, *Phys. Rev. B* **38**, 5547 (1988).

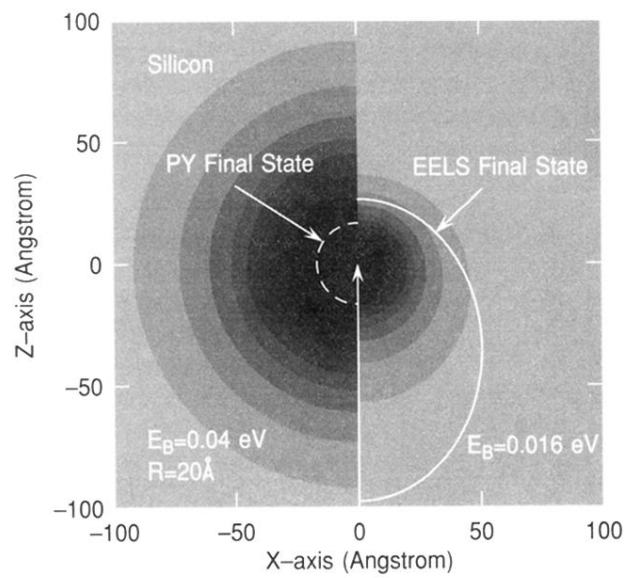


FIG. 2. Composite contour plot of total potential well with the swift electron (right) and without (left). The contours at half height for the first bound-state orbitals are shown as white lines. In the presence of the swift electron and wake, the orbital is larger and distorted towards the trailing correlation hole.